Redefining conventional biomass hydrolysis models by including mass transfer effects. Kinetic model of cellulose hydrolysis in supercritical water.

Luis Vaquerizo [a], Nerea Abad Fernández [a], Rafael B. Mato [a], María José Cocero [a,*]

a) High Pressure Processes Group, Department of Chemical Engineering and Environmental Technology, University of Valladolid (Spain). Prado de la Magdalena s/n. 47011, Valladolid, Spain.

* Corresponding author. Tel: +34 983423174; fax: +34 983423013, mjcocero@iq.uva.es (M.J. Cocero)

E-mail addresses: lvaquerizo@iq.uva.es (L. Vaquerizo), nerea.abad@uva.es (N. Abad Fernández), rbmato@iq.uva.es (R.B. Mato), mjcocero@iq.uva.es (M.J. Cocero)

Abstract

Conventional kinetic models of cellulose hydrolysis in supercritical water do not accurately represent the operation with concentrated suspensions since they neglect the mass transfer effects. This work proposes a kinetic model which is able to reproduce cellulose hydrolysis at high concentrations providing the optimum reaction conditions to obtain nanocellulose particles and oligomers of controlled size. The basic idea of the model, which is applicable to other lignocellulosic materials, is that the hydrolysis of the cellulose particles generates an oligosaccharides layer which creates a mass transfer resistance. Therefore, it considers both the diffusion of the water molecules from the bulk phase to the surfaces of the cellulose particles and the superficial hydrolysis kinetics. Experimental points were obtained working with two different cellulose types (*Dp* = 75µm and *Dp* = 50µm) at 390ºC and 25MPa, residence times between 50ms and 250ms and initial cellulose suspension concentration from 3% to 7% w/w (1% to 2.3%

w/w at the inlet of the reactor). The average deviation between the experimental points and the theoretical values is lower than 10% proving the applicability of the kinetic model. The experimental and theoretical results demonstrated that increasing the total number of cellulose particles, either increasing the initial concentration or decreasing the average particle diameter, reduces the hydrolysis rate.

Declarations of interest: None

Keywords

Mass transfer, Shrinking Core Model, particle surface, oligosaccharides layer, covering conversion.

1. Introduction

Replacing chemical and petrochemical industries by green technologies requires first redefining the conventional synthesis routes of the chemical compounds demanded by the society [1–6]. Adapting the production techniques to bio-based feedstocks implies moving from traditional organic synthesis to hydrolysis [7].

Unlike in traditional organic chemistry in which the chemical compounds are synthesized starting from simple molecules and aggregating functional groups, the obtaining of chemicals from biomass is commonly based, as a first step, on its hydrolysis to fundamental compounds [8]. Although biomass already contains all those functional groups, controlling the extension of the hydrolysis reaction, this is the degree of division of the biomass constituents, is still a challenge whose resolution is based on a deep understanding of the hydrolysis mechanisms and on the control of the reaction

conditions. An accurate control of the reaction time will allow selecting either the final hydrolysis compounds or the degree of polymerization of the biopolymers obtained from biomass hydrolysis. The combination of hydrolysis bioproducts and biopolymers in different proportions will create new biomaterials whose properties will fit the requirements demanded by the technological applications of today's society.

Although the acid and the enzymatic hydrolysis have been always considered the reference techniques in biomass hydrolysis [9,10], some disadvantages have penalized their fully implantation. Apart from the low selectivity, the long reaction times and the consequent increase of the equipment capacities, joined to the generation of residual effluents, demand a robust alternative.[8] In this context, biomass hydrolysis by hot pressurized water provides an opportunity to improve the current biomass hydrolysis standards. While the process selectivity is drastically increased reaching values over 90%, the reduction of the reaction time from minutes to milliseconds intensifies the process. Consequently, compared to traditional acid and enzymatic hydrolysis, the reduction of the equipment volumes from cubic meters to cubic centimeters allows delocalizing the process and exploit local biomass. Finally, the generation of residual effluents is greatly limited since only water is used as a reagent. [7,11]

The physical properties of supercritical water, water above its critical point (374ºC, 22MPa), can be finely tuned controlling the reaction conditions [11,12]. While its low dielectric constant, similar to the one of non-polar organic solvents, enhances the solubility of organic compounds, its low viscosity and high diffusivity improve the penetration of the water molecules into the lignocellulosic matrix. Finally, the possibility of easily modifying the dissociation of the water molecules varying the reaction conditions allows promoting either the ionic or the radical reactions and controlling the reaction pathways. [13]

Although the final step in the development of the bio-based industry shall be the direct processing of lignocellulosic biomass [14], its complexity joined to the drastic reaction conditions requires first understanding the mechanisms which govern the hydrolysis of its main constituents. Compared with lignin, an unstructured network of phenolic compounds, and with hemicellulose, a polysaccharide created by the combination of different monomeric units, cellulose is the simplest constituent of biomass [8]. Cellulose is a linear polysaccharide consisting on several glucose units linked by β-1,4 glycosidic bonds. Its degree of polymerization, which varies from several hundred to many thousands glucose units, depends on the raw material [12,15]. The aggregation of these saccharides chains, connected by hydrogen bonds created between the OH groups, form a three dimensional structure of fibrils characterized by its toughness and water insolubility [16–21]. Understanding cellulose hydrolysis mechanisms will provide a clear insight of biomass transformation fundamentals.

Traditionally, the main challenge linked to cellulose hydrolysis by supercritical water has been the operation with concentrated suspensions. Commonly, when working with cellulose suspensions, clogging problems both in the pumps and in the lines are faced. Overcoming the technical limitations which avoid a robust operation of the hydrolysis plants with concentrated suspensions will upgrade the technology resulting in a reduction of the capital and of the operating costs. Operating supercritical water hydrolysis plants with concentrated suspensions does not only reduces the size of the pieces of equipment involved in the process but decreases the energetic demand of the downstream process [22]. In this context, the majority of cellulose hydrolysis works have been based on low concentrated suspensions [12,23]. Although authors were aware of the fact that the substitution of traditional acid and enzymatic hydrolysis by supercritical water hydrolysis is greatly dependent on increasing the concentration of

the initial suspension, in the first hydrolysis works, understanding both the cellulose hydrolysis mechanism and the reaction pathways and obtaining the optimum reaction conditions was a priority. Consequently, because of the operating conditions, these works proposed simple kinetic models which consider that the cellulose particles are instantaneously dissolved and that hydrolysis is performed in a homogeneous phase [24–26]. The main outcome of these works is the definition of the cellulose hydrolysis pathways explaining how cellulose and its subsequent hydrolysis products are transformed when they are subjected to hydrolysis. Once dissolved, cellulose is hydrolyzed to long oligosaccharides chains which are then hydrolyzed to glucose. Finally, if hydrolysis proceeds, degradation products such as acids are obtained from glucose hydrolysis [27,28].

Once that the cellulose hydrolysis pathways have been explained and that the optimum reaction conditions have been adjusted, experimental works which analysed the effect of an increase of the cellulose suspension concentration have been performed [15]. These works proved that when the cellulose concentration is increased, even when the water mass concentration remained over 90%, a solid fraction remains unreacted. This fact demonstrates that the cellulose particles are not always fully dissolved in supercritical water. This evidence disagrees with the bases of the conventional hydrolysis models and explains the divergences between the experimental and the theoretical results found in these works. Therefore, when working with concentrated suspensions, neither dissolution can be considered as instantaneous nor hydrolysis understood as a process performed in a homogeneous phase. These two considerations neglect the cellulose step dissolution and the mass transfer effects. Although the conventional models are not able to predict cellulose hydrolysis at high concentrations, they must be the base to understand how the initial concentration influences cellulose hydrolysis.

In this work a kinetic model which accurately predicts cellulose hydrolysis at high concentrations is presented. The model, which considers the mass transfer effects, is based on the idea that the hydrolysis of the cellulose particles generates oligosaccharides which are instantaneously dissolved in the liquid phase and, because of their low diffusion coefficient, they remain as a layer which surrounds the cellulose particles creating a mass transfer limitation. Moreover, it considers that an increase in the cellulose concentration reduces the accessibility of the water molecules to the surface of the cellulose particles because of the higher probability of interaction between the oligosaccharides layers of the different particles (more particles are fed to the reactor) and because of the higher concentration of hydrolysis products in the aqueous phase. These compounds directly interact with the water molecules penalizing their diffusion to the surface of the cellulose particles.

Finally, although in the case of compounds such as hemicelluloses and lignin it can be also considered that their hydrolysis products can create a mass transfer resistance, because of their higher complexity, the model would need to be adapted and partially reformulated to represent the hydrolysis of natural biomasses.

2. Materials and Methods

2.1 Materials

Deionized water and two different types of high purity microcrystalline cellulose were selected to perform the validation experiments. While the first type of cellulose, with an average particle diameter of 50 µm was purchased from Sigma-Aldrich (Avicel® PH-101), the second one, with an average particle diameter of 75µm, was purchased from VWR (A17730). The standards used in the high-performance liquid chromatography (HPLC) analysis were: cellobiose (C98%), glucose (C99%), fructose (C99%), erythrose

(C75%), glyceraldehyde (C95%), glycolaldehyde dimer (C99%) and 5-hydroxymethylfurfural (C99%) purchased from Sigma. Sulfuric acid (C96%) and calcium carbonate (C99%) supplied by Sigma were used as reagents in the determination of structural carbohydrates. Milli-Q water was also used in this procedure.

2.2 Analysis

The solid fraction at the outlet of the reactor, which represents the unconverted cellulose, was determined by gravimetric analysis. This fraction was immediately separated by centrifugation from the product samples, dried at 60ºC during 24 hours and finally weighted. Then, cellulose conversion in the reactor was determined by Equation 1:

Equation 1: $$X = \frac{W_0 - W}{W_0}$$

Where X represents cellulose conversion, W_0 the cellulose mass concentration at the inlet of the reactor (g cellulose / g total) and W the cellulose mass concentration at the outlet of the reactor (g cellulose / g total).

The composition of the liquid product was determined by HPLC analysis. The column used for the separation of the compounds was Shodex SH-1011 at 50ºC, using sulfuric acid (0.01 N) as mobile phase with a flow rate of 0.8 ml/min. The Waters IR Detector 2414 was used to identify the sugars and their derivatives, and a Waters UV-Vis detector was used to determine the 5-hydroxymethylfurfural (5-HMF) concentration at a

wavelength of 254 nm. The concentration of soluble oligosaccharides in the liquid samples was determined by acid hydrolysis to glucose and HPLC determination following a laboratory analytical procedure from NREL (Sluiter et al [29]) as follows. To 10 ml of filtered liquid aliquots, 4 ml of 96 % H_2SO_4 was added. The sample was maintained in an oven at 30ºC for 60 min. Then 86 ml of Milli-Q water was added, and the sample was incubated at 121ºC for 60 min. Calcium carbonate was added to 20 ml of this sample to neutralize the pH, and finally the supernatant liquid was filtered and analysed by HPLC. Two replicates of each experiment were analysed in order to obtain reliable results.

The mass fraction of oligosaccharides in the liquid phase was determined by Equation 2, where *Col,c* and *Ccel,c* represent the concentration of oligosaccharides and the concentration of cellulose in the liquid phase on a carbon basis. The monomer was not considered as an oligosaccharide and therefore its mass fraction was subtracted. The carbon factors used to convert the concentrations of oligosaccharides and of cellulose into a carbon basis are 0.4 and 0.444 respectively. While *Col,c* is determined by HPLC following the Sluiter et al [29] method, *Ccel,c* is determined by Equation 3:

Equation 2: $$x_{ol} = \frac{C_{ol,C}}{C_{cel,C}}$$

Equation 3: $$C_{cel,C} = C_{cel,0} \cdot X$$

Where *Ccel,o* represents the cellulose concentration at the inlet of the reactor and *X* the cellulose conversion calculated by Equation 1.

Finally, the crystallinity of the samples was determined by XRD (X-Ray Diffraction) using a Bruker Discover D8 diffractometer in the Laboratorio de Técnicas Instrumentales of the University of Valladolid. The X-ray source is a copper tube, Cu Kα radiation (λ = 1.5418 Å), of 2.2 kW power which works at 40kV and 30 mA and which uses an energy dispersive type detector Lynxeye (Bruker) model. The measuring range, 2θ, variated from 10º to 45º with a step size of 0.02º and a time per step parameter of 1s. While the total number of steps was equal to 1713, the total measuring time was approximately equal to 31 minutes.

2.3 Experimental Setup

All the experiments were carried out in the FASTSUGARS continuous pilot plant designed and built by our research group [12]. A pressure of 25MPa and a temperature of 390ºC were selected as reaction conditions and fixed at the inlet of the reactor. Since the objective of the experiments is the validation of the cellulose consumption model, the residence time was varied from 50ms to 350ms in order to obtain the evolution of the cellulose consumption with the reaction time. Finally, the influence of the initial cellulose concentration was tested processing different cellulose suspension (3%, 5% and 7% w/w, 1%, 1.7% and 2.3% w/w at the inlet of the reactor). The process flow diagram of the pilot plant is shown in Figure 1:

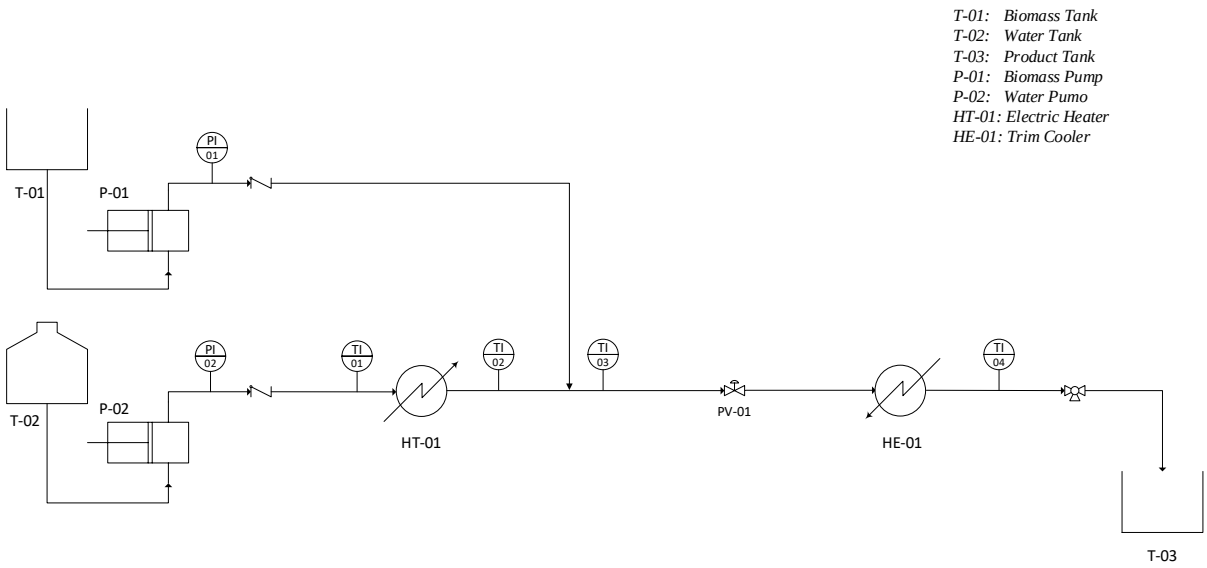

Figure 1: Experimental setup: FASTSUGARS pilot plant

In the FASTSUGARS pilot plant, two positive displacement pumps (P-01 & P-02) continuously pump from their storage tanks (T-01 & T-02 respectively) the biomass suspension and water up to the reaction pressure (25MPa). The process flows can be controlled modifying the pumped volume of the positive displacement pumps up to 3 kg/h in the case of the biomass suspension pump and up to 5 kg/h in the case of the water pump. The water stream is heated over its critical point using an electric heater (HT-01) with a design power of 10kW. After mixing both streams in a tee, the temperature is measured and controlled selecting as set point the reaction temperature (390ºC). The controller acts over the power released by the electric heater modifying the water stream temperature. Then the mixture enters in the reactor, which is basically a tube. The reaction time, calculated as the reactor volume divided by the volumetric flow of the inlet stream, is controlled varying either the initial flows or the reactor volume. In these experiments, reactors of an external diameter of 1/8” and different lengths were used. After the reactor, an expansion valve instantaneously stops the hydrolysis reactions decreasing the pressure from the reaction pressure (25MPa) to the atmospheric

pressure which, as a consequence of the Joule-Thompson effect, reduces the temperature instantly to 100ºC. Finally, the product stream is cooled down to 25ºC in the trim cooler exchanger (HE-01) and stored in the product tank (T-03). A three ways valve located just before the product tank allows taking product samples when desired.

3. Kinetic model

A recent work on cellulose hydrolysis [15] has demonstrated that when the cellulose concentration is increased over 1.5% w/w at the inlet of the reactor at 400ºC and 25MPa, a solid residue is obtained after hydrolysis. The model presented in this manuscript is based on two ideas which are in accordance with these results. It considers that the dissolution of a solid particle of cellulose is not an instantaneous process and that cellulose hydrolysis is a heterogeneous process governed by the cellulose dissolution velocity which is lower than the cellulose hydrolysis velocity. Thus, when hydrolysis starts, there is still a fraction of undissolved cellulose in solid state. Therefore, it is concluded that a mass transfer limitation, which becomes more relevant as the initial cellulose concentration is increased, governs cellulose dissolution. Traditional cellulose hydrolysis models [12,23] have been based on the Shrinking Core Model [30]. Specifically, in the approach which considers that once that the liquid molecules reach the solid particles, the reaction is produced on their surface decreasing the solid mass. However, since the dissolution is considered as an instantaneous stage, the mass transfer resistance has been neglected and only the hydrolysis stage has been considered. Therefore, these models consider the hydrolysis as a homogeneous process carried out in the aqueous phase. The model presented in this paper is also based on this approach of the Shrinking Core Model, but considering both the mass transfer and the

reaction stages. Cellulose particles are modelled as spheres whose diameter decreases as reaction proceeds. Although the traditional cellulose hydrolysis models [12,23] have modelled the cellulose fibers as cylinders instead of as spheres, in this model spheres have been considered. As demonstrated by Sasaki [23], as the cellulose hydrolysis proceeds, these long fibers are subjected to cleavage generating short cylinders. As the length of a cylinder is reduced, its external surface, parameter which quantifies the exposure of a cellulose particle to the water molecules, approaches to the external surface of a sphere. Moreover, in a short cylinder it is not possible to define whether the reduction in the size is produced in the radial or in the axial direction while in a sphere it is always produced in the radial direction. Therefore, taken into account these two considerations, the cellulose particles are modelled as spheres (although physically they are similar to short cylinders) reducing the complexity of the model.

In this model, cellulose hydrolysis is produced on the surface of the particles instead of in the aqueous phase. Then, the hydrolyzed compounds are instantaneously dissolved in the aqueous phase where their hydrolysis proceeds. Since the particle surface, which increases as the initial particle diameter increases, is directly related to the hydrolysis rate, using cellulose varieties with a high initial average particle diameter will increase the hydrolysis rate.

If it is considered that once that the water molecules reach the surface of the solid particles the hydrolysis is instantaneously performed, the mass transfer limitation must affect to the diffusion of the water molecules from the bulk phase to the surface of the solid particles. Focusing on the hydrolysis pathway, the first product obtained in cellulose hydrolysis are long oligosaccharides chains [12,31]. In this new model, these oligosaccharides chains are considered to be the responsible of the mass transfer limitation. Because of their high degree of polymerization and consequently, their great

length, the diffusion of the oligosaccharides chains to the bulk phase must be greatly limited. These chains are visualized surrounding the cellulose particles and therefore, creating a limitation to the arrival of more water molecules to the surface of the solid particles. Once that the oligosaccharides are hydrolyzed to short monosaccharides which can easily diffuse to the bulk phase, the limitation disappears and the water molecules are able to diffuse again to the solid cellulose particles. However, the cellulose hydrolysis produces new oligosaccharides chains which create again a mass transfer limitation. If the hydrolysis velocity of the solid particles is higher than the oligosaccharides hydrolysis velocity, the solid cellulose will be at some points of the process almost completely covered by oligosaccharides and the hydrolysis of the solid particles will be greatly limited. Although some authors [23] have proven that the viscosity average degree of polymerization of the solid residue after hydrolysis varies between 230 and 50, which can be considered as reference values to define a high polymerization degree, the model is based on the assumption of a low diffusion coefficient of the oligosaccharides chains instead of on the analysis of their effect depending on this parameter. The average degree of polymerization is constantly varying as the hydrolysis proceeds because of the generation of new oligosaccharides of a high polymerization degree and the hydrolysis of the ones which have been already dissolved in the liquid phase.

Finally, in this model it has been considered that all the cellulose particles have the same size and that the hydrolysis of one particle is representative of the hydrolysis of all the particles. Moreover, it is assumed that in cases in which the cellulose particle size distribution is not unimodal, the hydrolysis consumption can be modelled by means of the mean particle diameter. Therefore, all the equations presented hereafter are based on the hydrolysis of a single particle. Then, the total rate of cellulose consumption can be

easily obtained multiplying the consumption rate of one particle by the number of particles. A descriptive representation of the model is shown in Figure 2:

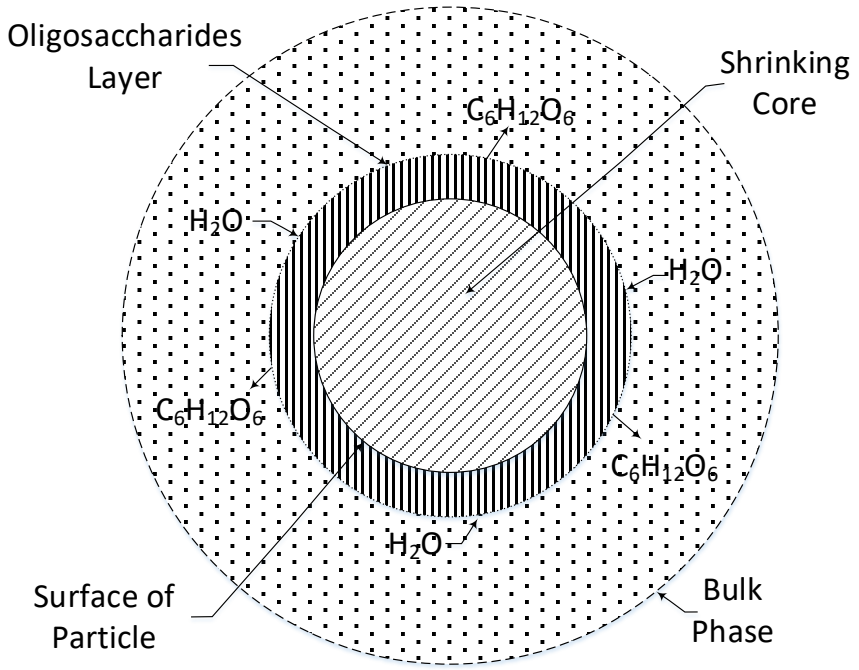

Figure 2: Representation of the cellulose hydrolysis model presented in this paper.

Once that the theoretical basis of the model have been explained, the main equations required to calculate the cellulose hydrolysis rate are presented hereafter. An extended and more detailed mathematical description of the equations can be found in the Supplementary Material of this work.

Reaction

The cellulose hydrolysis reactions are carried out on the surface of the solid cellulose particles once that the water molecules have diffused from the bulk phase:

Equation 4: $$-\frac{\mathrm{dNa}}{\mathrm{dt}} = \mathrm{kr} \cdot 4 \cdot \pi \cdot \mathrm{r}^2 \cdot \mathrm{Cai}$$

Where *–dNa/dt* represents the consumption of water on a mole basis, *kr* the kinetic constant, *r* the particle radius and *Cai* is the water molar concentration in the interphase between the solid particle and the aqueous phase.

Mass transfer

The water molecules are transferred from the bulk phase to the surface of the cellulose particles:

Equation 5: $$-\frac{\mathrm{dNa}}{\mathrm{dt}} = \mathrm{kg} \cdot 4 \cdot \pi \cdot \mathrm{r}^2 \cdot (\mathrm{Cag} - \mathrm{Cai})$$

As in the reaction term, *–dNa/dt* represents the consumption of water on a mole basis, *kg* is the mass transfer coefficient, *r* the particle radius, *Cai* is the water molar concentration in the interphase between the solid particle and the aqueous phase, and finally *Cag* is the water concentration in the bulk phase.

The continuity of the process requires that all the water molecules transferred from the bulk phase to the particle surface are consumed in the hydrolysis reactions. Then, equating Equation 4 and Equation 5:

Equation 6: $$\mathrm{Cai} = \frac{\mathrm{kg}}{\mathrm{kr}+\mathrm{kg}}\mathrm{Cag}$$

Equation 6 allows obtaining the value of the water interphase concentration. Replacing *Cai* in Equation 4:

Equation 7: $$-\frac{dNa}{dt} = 4 \cdot \pi \cdot r^2 \cdot \frac{kr \cdot kg}{kr+kg} \cdot Cag$$

Equation 7 allows calculating the water consumption independently of the water interphase concentration. Multiplying both terms of Equation 7 by the molecular weight of water, Equation 7 can be expressed on a mass basis as:

Equation 8: $$-\frac{dMa}{dt} = 4 \cdot \pi \cdot r^2 \cdot \frac{kr \cdot kg}{kr+kg} \cdot \rho a$$

Equation 8 quantifies the consumption of water in the cellulose hydrolysis process. The relationship between the cellulose consumption and the water consumption is defined by:

Equation 9: $$\frac{dMa}{dt} = \frac{1}{9} \cdot \frac{dMc}{dt}$$

Combining this relationship with Equation 8, it is possible to calculate the cellulose consumption rate on a mass basis:

Equation 10: $$-\frac{dMc}{dt} = 9 \cdot 4 \cdot \pi \cdot r^2 \cdot \frac{kr \cdot kg}{kr+kg} \cdot \rho a$$

The evolution of the particle radius during hydrolysis is easily obtained relating the particle mass with its corresponding volume:

Equation 11: $$r = \left(\frac{3}{4\cdot\pi}\cdot\frac{Mc}{\rho c}\right)^{1/3}$$

Where ρc is the particle density and Vc the particle volume.

The calculation of the cellulose hydrolysis rate by Equation 10 requires first calculating the values of the kinetic constant kr and of the mass transfer coefficient kg. Regarding the kinetic constant, kr, which is modelled as a pseudo-Arrhenius equation (Equation 12), two different correlations which depend on the reaction temperature have been proposed. These correlations are obtained using the kinetic constant of the model as a degree of freedom and adjusting its value to minimize the differences between the results predicted by the model and the results predicted by a conventional model [12]. Because of the low working concentrations (lower than 1% w/w at T=400ºC & P=25MPa) which were considered in the development of the conventional hydrolysis models, in this case it is possible to neglect the mass transfer effects.

Equation 12: $$kr = A\cdot\frac{\rho_{a,exp}}{\rho_a}\cdot\exp^{-\frac{Ea}{R\cdot T}}$$

Where kr is the kinetic constant, A is the preexponential factor, Ea is the activation energy, R is the universal gas constant, T the absolute temperature, $\rho_{a,exp}$ the density of water at the reaction conditions used to calculate the value of the preexponential factor and ρ_a the density of water at the desired reaction conditions.

The values thus obtained for the natural logarithm of the preexponential factor and of the activation energy are shown in Table 1:

T (ºC)	LnA	Ea (kJ/mol)
400	70,33	430,3
355	17,87	154,4

Table 1: Calculation of the kinetic constant *kr*. Pseudo-Arrhenius equation parameters: natural logarithm of the preexponential factor *LnA* and activation energy *Ea*.

Therefore, in the supercritical zone (temperatures above 375ºC), the kinetic constant is defined by:

Equation 13: $kr = \mathrm{Exp}(70.33) \cdot \frac{608.43}{\rho_{a,T}} \cdot \mathrm{Exp}\left(\frac{-430.3}{R \cdot T}\right)$

On the other hand, in the subcritical zone (temperatures below 375ºC), the kinetic constant is calculated by:

Equation 14: $kr = \mathrm{Exp}(17.87) \cdot \frac{166.54}{\rho_{a,T}} \cdot \mathrm{Exp}\left(\frac{-154.4}{R \cdot T}\right)$

Regarding the calculation of the mass transfer coefficient, *kg*, the Chilton-Colburn [32,33] analogy shown in Equation 15 has been considered:

Equation 15: $\frac{f}{2} = Sth \cdot Pr^{2/3} = Stm \cdot Sc^{2/3}$

Therefore, relating the momentum transfer with the mass transfer:

Equation 16: $$\frac{\mathrm{f}}{2} = \frac{\mathrm{kg}}{\mathrm{u}} \cdot \left(\frac{\mu}{\rho \mathrm{aDAB}}\right)^{2/3}$$

Where ρa, μ, D_{AB} are the density, the viscosity and the water diffusion coefficient calculated at the reaction conditions, u is the fluid velocity, f is the Darcy-Weisbach friction factor [34] and kg the mass transfer coefficient. The friction factor is directly calculated solving the Swamee and Jain equation [35]:

Equation 17: $$\mathrm{f} = \frac{0.25}{\left[\mathrm{Ln}\left(\frac{\varepsilon}{3.7\mathrm{D}} + \frac{5.74}{\mathrm{Re}^{0.9}}\right)\right]^2}$$

Where ϵ is the pipe roughness and D the pipe diameter.

Regarding the diffusion coefficient, D_{AB}, the value of this parameter is approached to the self-diffusion coefficient of water.

Once that the physical properties of water, the velocity and the friction factor are calculated, the value of the mass transfer coefficient is obtained solving Equation 16.

Finally, although the values of both the kinetic constant and of the mass transfer coefficient can be directly calculated and replaced in Equation 10, it is first necessary to include the limitation created by the oligosaccharides layer which surrounds each cellulose particle penalizing the water diffusion from the bulk phase to the surfaces of

435 the particles. Consequently a new concept called the “covering mass” has been included
436 and it is presented hereafter:

437 The “covering mass” is the mass of oligosaccharides which almost completely cover the
438 cellulose particles creating a mass transfer resistance which limits their hydrolysis. This
439 parameter depends on the cellulose concentration, the external surface of the particles
440 and the cellulose density.
441 Because of the complexity of experimentally estimating the value of this parameter, in
442 the first set of experiments shown in Section 4, this parameter is used as a degree of
443 freedom. Therefore, its value is adjusted in order to minimize the deviations between
444 the experimental data and the data predicted by the model. Since the mass of a single
445 cellulose particle can be even lower than 10^{-11} kg, in order to facilitate operating with
446 the model, the concept of “covering conversion” has been defined. The covering
447 conversion is simply the relationship between the oligosaccharides covering mass and
448 the initial mass of a cellulose particle:
449
450 Equation 18: $$X_{cov} = \frac{m_{olig}cov}{m_{cel}0}$$
451
452 Theoretical relationships between the covering conversions of different scenarios based
453 on the particle concentration and their external surface have been proposed. These
454 relationships allow calculating the value of the covering conversion of a real scenario
455 from a reference value of another scenario. The following relationships have been found
456 to accurately predict the value of the covering conversion within different scenarios:
457
458 - Same concentration, different cellulose:

Equation 19: $X_{cov}2 = \frac{Dp_2}{Dp_1} \cdot X_{cov}1$

Where Dp_1 and Dp_2 are respectively the diameter of the particles of the first and of the second scenarios.

- Same cellulose, different concentration:

Equation 20: $X_{cov}2 = \frac{Dpfic_1}{Dpfic_2} \cdot X_{cov}1$

Where *Dpfic* represents the fictitious diameter obtained if it is considered that the cellulose particles are grouped together in a single spherical particle (the total mass of the spherical particle is the sum of all individual particles masses).

The oligosaccharides consumption rate, which is required to calculate the mass of oligosaccharides in the liquid phase, is defined by Equation 21:

Equation 21: $\frac{dMol}{dt} = F \cdot \frac{dMc}{dt} - kol \cdot Mol$

The variation of the oligosaccharides mass is equal to the generation of oligosaccharides, defined as the fraction of cellulose hydrolyzed to oligosaccharides (*F*) multiplied by the cellulose consumption rate, minus the consumption of

oligosaccharides defined as a kinetic constant multiplied by the oligosaccharides mass. Both the values of *F* and *kol* have been already experimentally determined in a previous work of our research group [12]. In this case the kinetic constant, *kol*, follows a conventional Arrhenius equation. The values of *F* and of the kinetic parameters of *kol* are detailed in Table 2:

T (ºC)	F	LnA	Ea (kJ/mol)
>350	0.8	25.4	135.2

Table 2: Oligosaccharides production Factor *F* and Arrhenius equation parameters: natural logarithm of the preexponential factor *LnA* and activation energy *Ea*. [12]

With these two considerations, Equation 16 is redefined again:

Equation 22: $$\mathrm{kg} = \frac{\mathrm{f}}{2} \cdot \frac{\mathrm{u}}{\left(\frac{\mu}{\rho \cdot \mathrm{DAB}}\right)^{2/3}} \cdot (1 - \mathrm{frac})$$

Where (1 – *frac*) models the mass transfer limitation created by the oligosaccharides layer and the hydrolysis products. "*frac*" is the relationship between the value of the oligosaccharides mass (calculated solving Equation 21) and the covering mass. Thus, when the covering mass is reached, *frac* is equal to 1 and *kg* is equal to 0.

Equation 22 allows calculating the mass transfer coefficient that, in combination with the value of the kinetic constant *kr* calculated by Equation 13 and Equation 14, provide the cellulose consumption rate.

4. Results and Discussion

The validation of the model has been performed comparing three sets of experimental data with the results predicted by the kinetic model. The concept of absolute average deviation, defined by Equation 23, has been used to quantify the errors between the experimental and the theoretical values:

Equation 23:

$$absolute\ average\ deviation = \frac{1}{N} \cdot \sum_{i=0}^{n} \left(\frac{\text{Theoretical Value} - \text{Experimental Value}}{\text{Theoretical Value}} \right) \cdot 100$$

Where *N* represents the number of experimental points.

4.1 Covering conversion. Adjustment of a reference value.

The application of the kinetic model presented in this manuscript requires as a first step to calculate in each scenario the value of the covering conversion, parameter which depends on the cellulose type and on the initial cellulose concentration. The covering conversion of any working scenario can be easily calculated applying Equation 19 and Equation 20 once that the covering conversion associated with any other scenario (cellulose type and initial concentration) is known. Since the kinetic model has not been previously applied, there is no value of the covering conversion available to be considered as a reference. Therefore, the first set of experimental data has been used to

manually adjust the value of this parameter to the one which minimizes the discrepancies between the experimental points and the values predicted by the kinetic model. This covering conversion will later be used as a reference to calculate the values of the covering conversions of the following scenarios. If the theoretical results predicted by the model in the following cases are in agreement with the experimental data, both the kinetic model and the covering conversion adjusted in this section will be validated.

In this base case, VWR cellulose was used (*Dp* = 75µm). The initial cellulose suspension concentration was fixed at 5% w/w, 1.7% w/w at the inlet of the reactor, because of the dilution produced when the suspension stream is mixed with the supercritical water stream. In all the experiments performed with this working concentration solid residue was obtained. Therefore, the cellulose dissolution cannot be consider as instantaneous and the model presented in this work was applied. Figure 3 compares the evolution of the cellulose conversion predicted by the model once that the covering conversion has been manually adjusted with the experimental data:

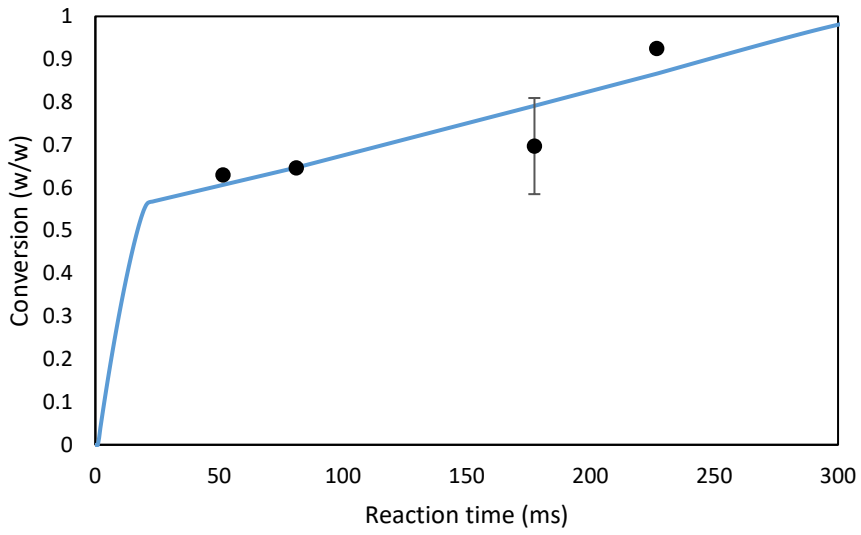

Figure 3: Adjustment of the covering conversion. Initial cellulose suspension concentration 5% w/w, 1.7% w/w at the inlet of the reactor. Particle diameter, *Dp* = 75µm. (●) Experimental results. (—) Theoretical results fitted by the kinetic model presented in this article.

The deviations between the experimental data and the theoretical values have been quantified and are presented in Table 3:

Experimental Value	Calculated Value	Abs Avg Dev (%)
0.63	0.61	3.6
0.65	0.65	0.0
0.70	0.79	13.4
0.93	0.87	6.6
	Avg Deviation (%)	5.9

Table 3: Absolute average deviations between the experimental conversion data and the theoretical values fitted by the kinetic model. Adjustment of a reference value of the covering conversion.

As it can be seen from Figure 3 and Table 3, the discrepancies between the experimental and the theoretical values have been minimized adjusting the covering conversion to 0.44. The absolute average deviation between the experimental and the theoretical points is lower than 6%. Thus, this working scenario which is summarized as cellulose concentration equal to 1.7% w/w at the inlet of the reactor, particle diameter, *Dp* = 75µm and covering conversion X_{cov} = 0.440, will be used as reference.

As it can be seen from Figure 3, the model predicts two different hydrolysis zones. This is the main difference with the conventional cellulose hydrolysis models [12,15,23] in which the cellulose hydrolysis is represented by means of a continuous equation. In the first zone, which are basically the first twenty five milliseconds of reaction, the water molecules are able to easily react with the cellulose particles on their surface because of the low concentration of oligosaccharides in the aqueous phase and consequently, the low mass transfer resistance. In this initial phase, the conversion of the cellulose particle rises drastically up to a 60%. Therefore, according to this model, during this initial period of direct reaction between the water molecules and the cellulose surface there is a minimum cellulose conversion value which is limited by the minimum reaction time which can be technically achieved.

After these first milliseconds, the cellulose hydrolysis rate is reduced because of the increase of the oligosaccharides concentration in the liquid phase. According to the model, controlling the reaction time in this second zone will allow obtaining oligosaccharides chains of different length. While operating close to the first reaction zone (short reaction times) will provide long oligosaccharides chains, the operation with longer reaction times will provide short oligosaccharides chains. As the oligosaccharides are progressively hydrolyzed and new pathways to the cellulose surface are opened, the cellulose hydrolysis proceeds. Since the hydrolysis of the cellulose particle generates again more oligosaccharides chains, the hydrolysis of the particle is slowed down again until the new oligosaccharides chains are hydrolyzed to sugars and acids which can easily diffuse to the bulk phase. These two processes (first the hydrolysis of the cellulose particle and the covering of the particle, and then the hydrolysis of the oligosaccharides chains) reach an equilibrium resulting in a constant hydrolysis rate which lasts until the total consumption of the cellulose particle which in

585 this case is produced after 300ms of hydrolysis. Finally, once that the solid particle has
586 been consumed, the hydrolysis of the oligosaccharides chains and sugar molecules
587 proceeds homogeneously in the aqueous phase and it is accurately modelled by the
588 conventional hydrolysis models [12,15,23].

589 The validation of the conclusions extracted from the application of the kinetic model to
590 the first set of experimental data has been performed experimentally determining the
591 selectivity of the sugars in the liquid phase and the crystallinity of the solid residues
592 obtained after the hydrolysis. On the one hand, the selectivity of sugars in the liquid
593 phase, which has been obtained by HPLC and it is presented in Figure 4, is used to
594 verify the basic idea of the model which states that the oligosaccharides chains are the
595 responsible of the mass transfer limitations in cellulose hydrolysis. On the other hand,
596 the crystallinity of the solid cellulosic residue, obtained by XRD and shown in Figure 5,
597 has been determined to confirm whether the solid residue obtained after hydrolysis is
598 crystalline or amorphous cellulose.

599

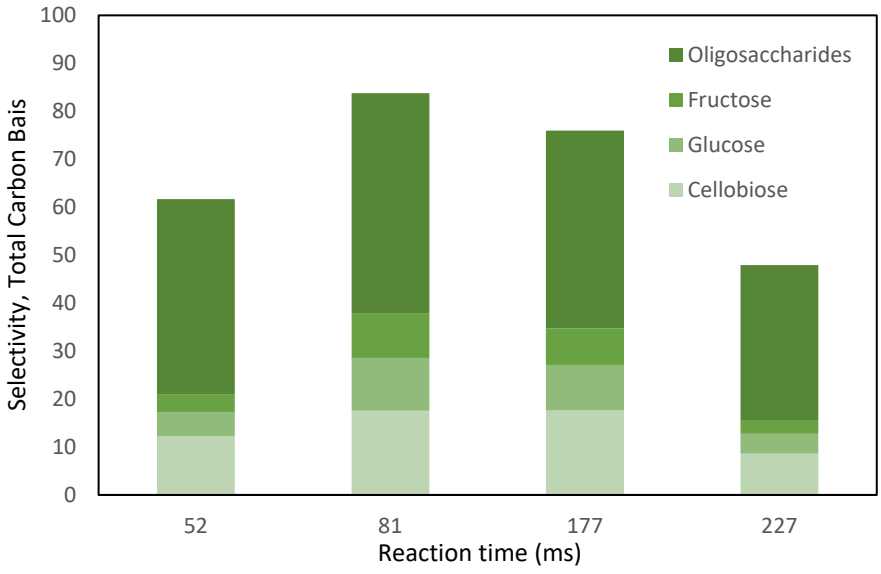

600

Figure 4: Selectivity of sugars in the liquid phase at different reaction times. Initial cellulose concentration 5% w/w, 1.7% w/w at the inlet of the reactor. VWR cellulose: particle diameter, *Dp* = 75µm.

As it can be seen from Figure 4, the selectivity of both the total saccharides and of the oligosaccharides increases up to a maximum of 84% in the case of the saccharides and up to 46% in the case of the oligosaccharides after 80 ms of hydrolysis. After this maximum, both selectivities decrease. This behaviour, which is very similar to the one reported by Cantero [36] in a previous work, explains the existence of two different hydrolysis zones. First, when no oligosaccharides have been generated and the effect of the mass transfer resistance is reduced, the cellulose hydrolysis rate is very high. Then, when both the concentration of oligosaccharides and the mass transfer resistance increase, a reduction in the cellulose hydrolysis rate is observed.

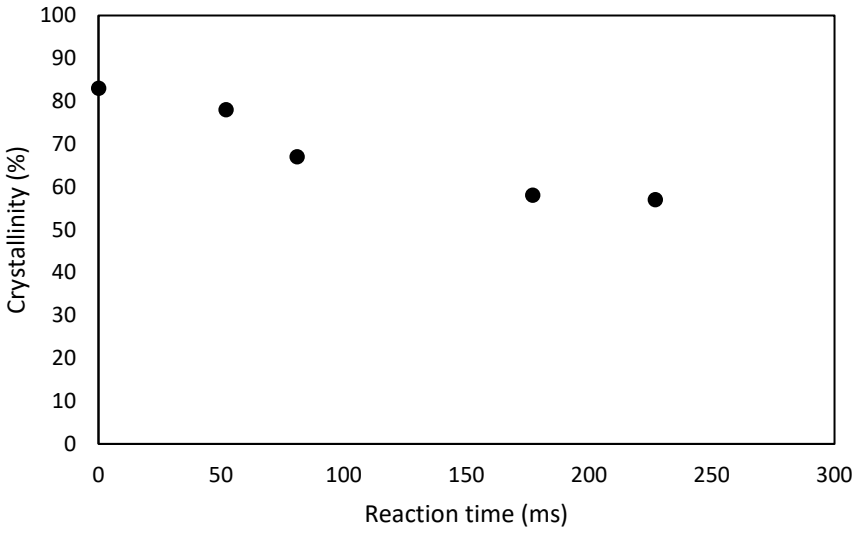

Figure 5: Analysis of the crystallinity of the cellulosic solid residue after hydrolysis. Initial cellulose concentration 5% w/w, 1.7% w/w at the inlet of the reactor. VWR cellulose: particle diameter, *Dp* = 75 µm.

Finally, regarding the crystallinity of the solid cellulosic residue and according to the results presented in Figure 5, the crystallinity of the solid cellulosic residue decreases as the reaction time increases. The experimental results show that after 230 ms of reaction, which means the almost complete hydrolysis of the cellulose particles, the crystallinity of the solid residue remains at 57%. Considering that the crystallinity of the initial cellulose is equal to 83%, a 31% of the initial crystalline zones have been converted into amorphous zones. Therefore, it is concluded that the obtaining of small cellulose particles has associated a reduction in their crystallinity. Although these results show a surprising tendency in the evolution of the crystallinity (as the hydrolysis proceeds, first the amorphous zones, easily accessible and more reactive, should be consumed increasing the crystallinity of the solid residue), some authors as Sasaki [23] and Deguchi [37] have already reported this behaviour. Moreover, Deguchi proved that around 320ºC, the crystalline cellulose I is converted into amorphous cellulose and then, after the hydrolysis, it recrystallizes into crystalline cellulose II. These amorphous transition and later recrystallization phenomena are considered as the base to explain this behaviour.

4.2 Model validation. Same cellulose different concentration.

In this section, the hydrolysis model presented in this manuscript is validated comparing a second set of experimental data with the theoretical values predicted by the kinetic model. Moreover, the influence of the initial cellulose concentration is analysed increasing this parameter up to 7% w/w, 2.3% w/w at the inlet of the reactor. The value of the covering conversion has been calculated considering as reference the value adjusted in Section 4.1. After calculating the fictitious diameters (considering that the

particles are grouped in a single spherical particle whose mass is equal to the sum of the masses of the single particles) and applying Equation 20, the calculated value of the covering conversion is equal to $X_{cov} = 0.376$. In this set of experiments, the same cellulose type as in Section 4.1 has been hydrolyzed (VWR cellulose, *Dp* = 75µm). Figure 6 shows the comparison between the evolution of the cellulose conversion predicted by the kinetic model and the experimental data:

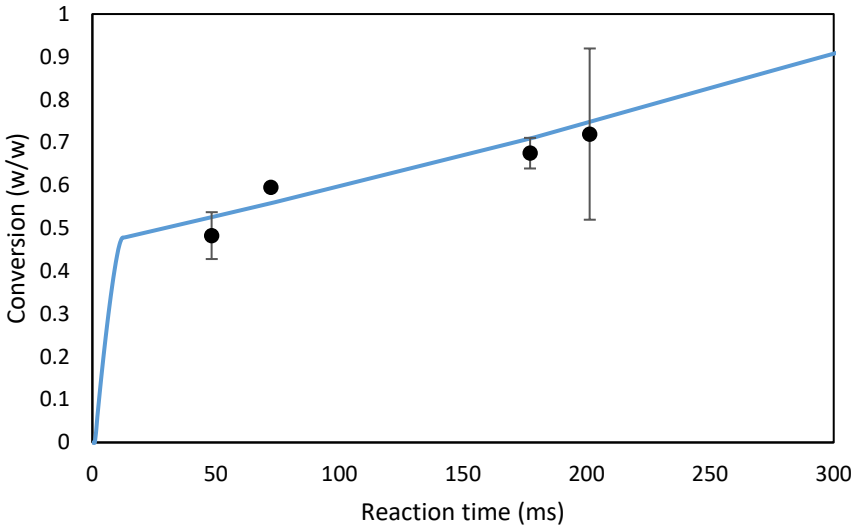

Figure 6: Model validation. Comparison between experimental data and theoretical values. Same cellulose, different concentration. Covering conversion equal to 0.376. Initial cellulose suspension concentration 7% w/w, 2.3% w/w at the inlet of the reactor. Particle diameter, *Dp* = 75µm. (●) Experimental results. (▬) Theoretical results predicted by the kinetic model presented in this article.

The deviations between the experimental data and the theoretical values have been quantified and are presented in Table 4:

Experimental Value	Calculated Value	Abs Avg Dev (%)
0.48	0.53	8.9
0.60	0.56	6.2
0.68	0.71	5.1
0.72	0.79	9.6
	Avg Deviation (%)	7.4

Table 4: Absolute average deviations between the experimental data and the theoretical values predicted by the kinetic model. Validation example, same cellulose, different concentration.

Since the average deviation is lower than 8%, it is proved that the theoretical results are in agreements with the experimental values. Therefore, the kinetic model, the value of the covering conversion adjusted in Section 4.1 and the relationship proposed in Equation 20 are validated. Comparing these results with the ones obtained in the base case presented in Section 4.1, the kinetic model predicts the same two hydrolysis zones but in this case, the value of the covering conversion is lower (0.376 vs 0.440) because of the influence of the initial cellulose concentration. Although one of the premises of this model is that the hydrolysis of a single particle is representative of the hydrolysis of the rest of the particles, this does not contradict the fact that the hydrolysis of each particle is influenced by the hydrolysis of the rest of the particles. Since the increase in the number of particles produces an increase in the total number of oligosaccharides chains and hydrolysis products in the aqueous phase, the diffusion of water molecules to the surface of the cellulose particles is more penalized because of the presence of these molecules and the interaction between the oligosaccharides chains of the different

678 particles. Thereby, the oligosaccharides generated in the hydrolysis of one particle also
679 interact with the surrounding particles. This phenomenon explains the reduction in the
680 value of the covering conversion. Finally, since the initial cellulose concentration has
681 been increased, the total cellulose hydrolysis time is higher than in the base case.

682

683 **4.3 Model validation. Different cellulose type.**

684

685 While in Section 4.2 the influence of the initial cellulose concentration has been
686 analysed, in this section the influence of the cellulose type is studied. In this case,
687 Avicel cellulose type, *Dp* = 50µm, has been selected to perform the experiments. Three
688 different experiments at suspensions concentrations of 3% w/w, 5% w/w and 7% w/w,
689 1%, 1.7% and 2.3% w/w at the inlet of the reactor have been carried out. Therefore, the
690 respective covering conversions are calculated applying Equation 19 and Equation 20.
691 After calculating the relationships between the particle diameters and the fictitious
692 diameters, the values of the covering conversions obtained are equal to 0.327 in the case
693 of 3% w/w suspension, 0.293 in the case of 5% w/w suspension and 0.250 in the case of
694 7% w/w suspension. Figure 7 shows the comparison between the evolution of the
695 cellulose conversions predicted by the kinetic model and the experimental data:

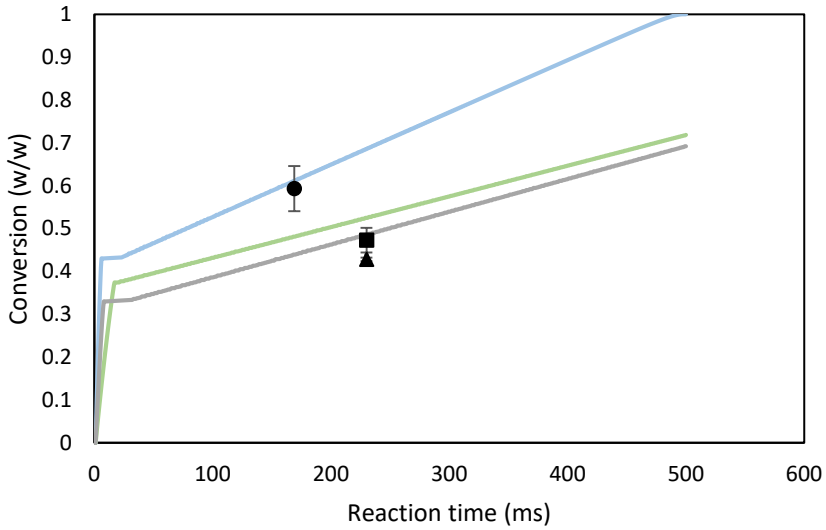

Figure 7: Model validation. Comparison between experimental data and theoretical values. Different cellulose type. Particle diameter, *Dp* = 50µm. (●, ■, ▲) Experimental data. Initial cellulose suspension concentration equal to 3% w/w (1% w/w at the inlet of the reactor), 5% w/w (1.7% w/w at the inlet of the reactor) and 7% w/w (2.3% w/w at the inlet of the reactor) respectively. (—, —, —) Theoretical results predicted by the kinetic model. Initial cellulose suspension concentration equal to 3% w/w (1% w/w at the inlet of the reactor), 5% w/w (1.7% w/w at the inlet of the reactor) and 7% w/w (2.3% w/w at the inlet of the reactor) respectively. Covering conversions equal to 0.327, 0.293 and 0.250 respectively.

The deviations between the experimental data and the theoretical values are presented in Table 5:

Concentration (%)	Experimental Value	Calculated Value	Abs Avg Dev (%)
3	0.59	0.61	3.0
5	0.47	0.52	11.0
7	0.43	0.49	13.4
		Avg Deviation (%)	9.1

Table 5: Absolute average deviations between the experimental data and the theoretical values predicted by the kinetic model. Validation example, different cellulose.

Since the absolute average deviation is lower than 10% the good agreement between the experimental results and the theoretical values validates the model, the covering conversion adjusted in Section 4.1 and the relationships proposed in Equation 19 and Equation 20. Since the particle diameter of the Avicel cellulose type is lower than that of the VWR type (50µm vs 75µm), a higher number of cellulose particles is expected. Consequently, as in the case presented in Section 4.2, the influence of the hydrolysis of one particle on the surrounding particles will be higher than in the base case reducing the value of the covering conversion. In this scenario, although the cellulose conversions after the first hydrolysis phase are lower than in the base case presented in Section 4.1 (45%, 35% and 30% with inlet suspension concentrations equal to 3% w/w, 5% w/w and 7% w/w respectively versus 60% in the base case), since the covering conversions are lower (0.327, 0.293 and 0.250 with inlet suspension concentrations equal to 3% w/w, 5% w/w and 7% w/w respectively versus 0.440), the second hydrolysis phase is longer in all cases. Because of the reduced value of the covering conversions, the particles are easily covered by the oligosaccharides layer, decreasing the cellulose consumption rate and increasing the total hydrolysis time.

Comparing the three cases presented in this section, as in Section 4.1 and Section 4.2 in which VWR cellulose has been used, increasing the initial cellulose concentration reduces the value of the covering conversion. Furthermore, in Figure 7 it is possible to appreciate the influence of the temperature in the hydrolysis model. While the temperature in the first experiment (suspension of 3% w/w) was equal to 396.3ºC, in the second and third experiments (suspensions of 5% w/w and 7% w/w) it remained at

384.8ºC and at 390.8ºC respectively. Increasing the temperature increases the kinetic constants *kr* and *kol* increasing the cellulose consumption rate. This reason explains the reduced separation between the curves of 5% w/w and 7% w/w (1.7% and 2.3% w/w at the inlet of the reactor) and the larger separation between the curves of 3% w/w and 5% w/w (1% and 1.7% w/w at the inlet of the reactor).

Finally, two additional experimental points available in literature [23] have been considered to validate the model with a different cellulose variety and a different reaction temperature (375ºC versus 390ºC). In this last case, the experimental points were obtained working with Merck cellulose, *Dp* = 50µm, and selecting a cellulose concentration at the inlet of the reactor equal to 2% w/w. Figure 8 shows the comparison between the evolution of the cellulose conversions predicted by the kinetic model and the experimental data:

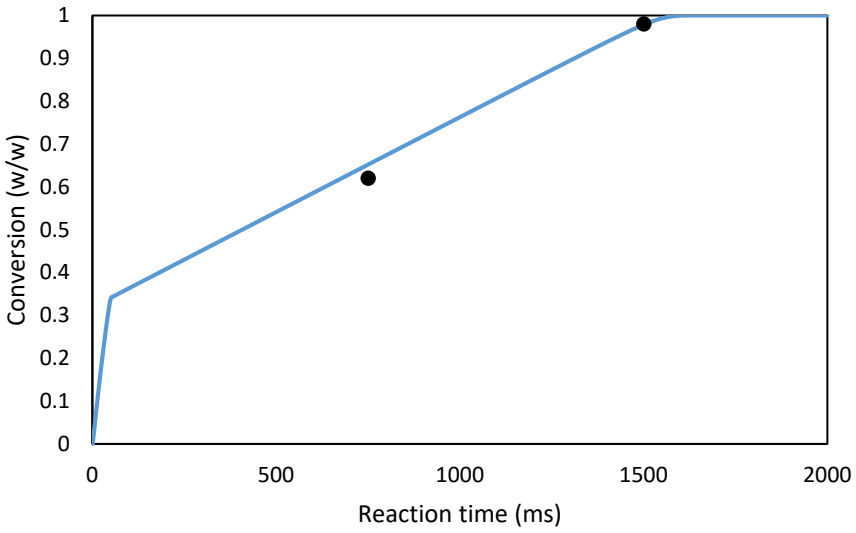

Figure 8: Model validation. Comparison between experimental data and theoretical values. Different cellulose type. Reaction temperature equal to 375ºC. Particle diameter, *Dp* = 50µm. Cellulose concentration at the inlet of the reactor equal to 2% w/w. (●) Experimental data [23]. (▬) Theoretical results predicted by the kinetic model. Covering conversion equal to 0.264.

The deviations between the experimental data and the theoretical values are presented in Table 6:

Experimental Value	Calculated Value	Abs Avg Dev (%)
0.62	0.65	5.2
0.98	0.98	0.2
	Avg Deviation (%)	2.7

Table 6: Absolute average deviations between the experimental data and the theoretical values predicted by the kinetic model. Validation example, different cellulose, reaction temperature equal to 375ºC.

As it can be seen from Figure 8 and Table 6, the good agreement between the experimental and the theoretical values validates the model when a different cellulose type and a different reaction temperature are considered. As the reaction temperature decreases, the values of the cellulose hydrolysis and oligosaccharides hydrolysis kinetic constants are reduced. Therefore, the cellulose hydrolysis rate decreases and the reaction time increases. As in the previous scenario and compared to the base case presented in Section 4.1, since the particle diameter is reduced from 75μm to 50μm and the cellulose concentration at the inlet of the reactor is increased from 1.7% w/w to 2% w/w, a higher number of particles is expected. Consequently, the covering conversion is reduced from 0.440 to 0.264 as well as the cellulose conversion after the first hydrolysis zone which decreases from 60% in the base case to 35% in the present case.

Finally, the arithmetic average of all the absolute average deviations shown in the three subsections of Section 4 has been calculated. Since this value is lower than 10% it is proved that the kinetic model presented in this manuscript is able to accurately

774 reproduce the cellulose hydrolysis process even when it is performed at a high initial
775 cellulose concentration and consequently, that it can be used to predict the optimum
776 reaction conditions required to obtain nanocellulose particles and oligomers of
777 controlled size.

778

779 ## 5. Conclusions

780

781 The conventional models of cellulose hydrolysis in supercritical water are limited to the
782 processing of low concentrated suspensions since they neglect the dissolution of the
783 cellulose particles and the mass transfer effects. In this work, a kinetic model which
784 accurately represents cellulose hydrolysis at high concentrations providing the optimum
785 reaction conditions to obtain nanocellulose particles and oligomers of controlled size
786 was presented. The model considers that the hydrolysis of the cellulose particles
787 generates oligosaccharides layers which create a mass transfer resistance.
788 The experimental and the theoretical results demonstrated that increasing the total
789 number of cellulose particles, either increasing the initial concentration or using a
790 cellulose variety with a smaller particle diameter, reduces the hydrolysis rate.
791 The kinetic model predicts two clearly differentiated hydrolysis zones. The first zone,
792 characterized by a fast cellulose hydrolysis rate and directly related with the low
793 oligosaccharide concentration, predicts that there is a minimum conversion value which
794 is limited by the minimum reaction time which can be technically achieved. On the
795 other hand, in the second hydrolysis region, the kinetic model predicts a lower cellulose
796 hydrolysis rate because of the higher oligosaccharides concentration.

797

798 **Acknowledgements**

799 The authors thank MINECO, Junta Castilla y León and FEDER program for the
800 financial support Projects CTQ2013-44143-R, CTQ2016-79777-R, and VA040U16.

801

802 **Nomenclature**

Abbreviation	Name	Units
Dp	Particle Diameter	m
ρp	Particle Density	kg/m^3
G	Gibbs Free Energy	J
H	Enthalpy	J
T	Temperature	K
S	Entropy	J/K
X	Conversion	dimensionless
Wo	Initial Cellulose Mass	kg
W	Cellulose Mass	kg
xol	Oligosaccharides Mass Fraction	dimensionless
Col,c	Oligosaccharides Concentration, Carbon Basis	ppm
Ccel,c	Cellulose Concentration, Carbon Basis	ppm
Ccel,o	Initial Cellulose concentration	ppm
Na	Water Moles	mol
t	Time	s
-dNa/dt	Water Consumption, Molar	mol/s
kr	Kinetic Constant	m/s
r	Particle Radius	m
Cai	Water Concentration, Interphase, Molar	mol/m^3
kg	Mass Transfer Coefficient	m/s

Cag	Water Concentration, Bulk Phase, Molar	mol/m^3
Ma	Water Mass	kg
-dMa/dt	Water Consumption Rate, Mass	kg/s
Mc	Cellulose Mass	kg
-dMc/dt	Cellulose Consumption Rate, Mass	kg/s
Mg	Glucose, Mass	kg
dMg/dt	Glucose Production Rate, Mass	kg/s
ρa	Water Density	kg/m^3
ρa,exp	Water Density in the calculation of A	kg/m^3
ρc	Cellulose Density	kg/m^3
Vc	Cellulose Volume	m^3
k	Kinetic Constant, Conventional Model	1/s
A	Preexponential Factor	dimensionless
Ea	Activation Energy	kJ/mol
R	Universal Gas Constant	J/mol·K
f	Darcy-Weisbach Friction Factor	dimensionless
Sth	Stanton Heat Number, Nu/Re·Pr	dimensionless
Pr	Prandtl Number	dimensionless
Stm	Stanton Mass Number, Sh/Re·Sc	dimensionless
Sc	Schmidh Number	dimensionless
Nu	Nusselt Number	dimensionless
Re	Reynolds Number	dimensionless
Sh	Sherwood Number	dimensionless
u	Velocity	m/s
ρ	Water Density	kg/m^3
μ	Water Viscosity	kg/m·s

D_{AB}	Water Diffusion Coefficient	m^2/s
ε	Pipe Roughness	m
D	Pipe Diameter	m
Xcov	Covering conversion	dimensionless
$m_{oligcov}$	Oligosaccharides Covering Mass	kg
m_{cel0}	Initial Cellulose Particle Mass	kg
Np	Particles Number	dimensionless
Dp_{fic}	Fictitious Particle Diameter	m
Mol	Oligosaccharides Mass	kg
-dMol/dt	Oligosaccharides Consumption Rate, Mass	kg/s
F	Cellulose Fraction Hydrolyzed to Oligosaccharides	dimensionless
kol	Oligosaccharides Consumption Kinetic Constant	1/s
frac	Oligosaccharides Mass / Covering Mass	dimensionless
N	Number of Experimental Points	dimensionless

References:

[1] J.A. Melero, J. Iglesias, A. Garcia, Biomass as renewable feedstock in standard refinery units. Feasibility, opportunities and challenges, Energy Environ. Sci. 5 (2012) 7393.

[2] M. Mascal, E.B. Nikitin, Direct, high-yield conversion of cellulose into biofuel, Angew. Chemie - Int. Ed. 47 (2008) 7924–7926.

[3] J.P. Meyer, P. Kozlowski, J. Jackson, K.M. Cunanan, P. Adumeau, T.R. Dilling, B.M. Zeglis, J.S. Lewis, Exploring Structural Parameters for Pretargeting Radioligand Optimization, J. Med. Chem. 60 (2017) 8201–8217.

[4] A.T. Martínez, How to break down crystalline cellulose, Science (80-.). 352 (2016) 1050–1051.

[5] Y. Zhao, W.-J. Lu, H.-T. Wang, Supercritical hydrolysis of cellulose for oligosaccharide production in combined technology, Chem. Eng. J. 150 (2009) 411–417.

[6] H. Pińkowska, P. Wolak, A. Złocińska, Hydrothermal decomposition of alkali lignin in sub- and supercritical water, Chem. Eng. J. 187 (2012) 410–414.

[7] K. Arai, R.L. Smith, T.M. Aida, Decentralized chemical processes with supercritical fluid technology for sustainable society, J. Supercrit. Fluids. 47 (2009) 628–636.

[8] M.J. Cocero, Á. Cabeza, N. Abad, T. Adamovic, L. Vaquerizo, C.M. Martínez, M.V. Pazo-Cepeda, Understanding biomass fractionation in subcritical & supercritical water, J. Supercrit. Fluids. 133 (2018) 550–565.

[9] C.-H. Zhou, X. Xia, C.-X. Lin, D.-S. Tong, J. Beltramini, Catalytic conversion of lignocellulosic biomass to fine chemicals and fuels, Chem. Soc. Rev. 40 (2011) 5588.

831 [10] M.R. Ladisch, C.M. Ladisch, G.T. Tsao, Cellulose to Sugars: New Path Gives
832 Quantitative Yield, Science (80-.). 201 (1978) 743–745.
833 [11] D.A. Cantero, M.D. Bermejo, M.J. Cocero, Governing Chemistry of Cellulose
834 Hydrolysis in Supercritical Water, ChemSusChem. 8 (2015) 1026–1033.
835 [12] D.A. Cantero, M.D. Bermejo, M.J. Cocero, Kinetic analysis of cellulose
836 depolymerization reactions in near critical water, J. Supercrit. Fluids. 75 (2013)
837 48–57.
838 [13] D.A. Cantero, Á. Sánchez Tapia, M.D. Bermejo, M.J. Cocero, Pressure and
839 temperature effect on cellulose hydrolysis in pressurized water, Chem. Eng. J.
840 276 (2015) 145–154.
841 [14] C.M. Piqueras, Á. Cabeza, G. Gallina, D.A. Cantero, J. García-Serna, M.J.
842 Cocero, Online integrated fractionation-hydrolysis of lignocellulosic biomass
843 using sub- and supercritical water, Chem. Eng. J. 308 (2017) 110–125.
844 [15] C.M. Martínez, D.A. Cantero, M.D. Bermejo, M.J. Cocero, Hydrolysis of
845 cellulose in supercritical water: reagent concentration as a selectivity factor,
846 Cellulose. 22 (2015) 2231–2243.
847 [16] A. Wang, T. Zhang, One-pot conversion of cellulose to ethylene glycol with
848 multifunctional tungsten-based catalysts, Acc. Chem. Res. 46 (2013) 1377–1386.
849 [17] L. Zhang, C. (Charles) Xu, P. Champagne, Overview of recent advances in
850 thermo-chemical conversion of biomass, Energy Convers. Manag. 51 (2010)
851 969–982.
852 [18] R.J. Moon, A. Martini, J. Nairn, J. Simonsen, J. Youngblood, Cellulose
853 nanomaterials review: structure, properties and nanocomposites, Chem. Soc. Rev.
854 40 (2011) 3941.
855 [19] Suhas, V.K. Gupta, P.J.M. Carrott, R. Singh, M. Chaudhary, S. Kushwaha,

Cellulose: A review as natural, modified and activated carbon adsorbent, Bioresour. Technol. 216 (2016) 1066–1076.

[20] D. Klemm, B. Heublein, H.P. Fink, A. Bohn, Cellulose: Fascinating biopolymer and sustainable raw material, Angew. Chemie - Int. Ed. 44 (2005) 3358–3393.

[21] A. Frey-wyssling, The fine structure of cellulose microfibrils, Science (80-.). 119 (1954) 80–82.

[22] L. Vaquerizo, M.J. Cocero, A Green Desuperheater for an Energetic Efficient Alternative to the Decompression Valve in Supercritical Water Hydrolysis Process. CFD Simulation, in: Comput. Aided Chem. Eng., 2017: pp. 2905–2910.

[23] M. Sasaki, T. Adschiri, K. Arai, Kinetics of Cellulose Conversion at 25 MPa in Sub- and Supercritical Water, AIChE J. 50 (2004) 192–202.

[24] Y. Ogihara, R.L. Smith, H. Inomata, K. Arai, Direct observation of cellulose dissolution in subcritical and supercritical water over a wide range of water densities (550-1000 kg/m3), Cellulose. 12 (2005) 595–606.

[25] L.K. Tolonen, M. Juvonen, K. Niemelä, A. Mikkelson, M. Tenkanen, H. Sixta, Supercritical water treatment for cello-oligosaccharide production from microcrystalline cellulose, Carbohydr. Res. 401 (2015) 16–23.

[26] K. Ehara, S. Saka, Decomposition behavior of cellulose in supercritical water, subcritical water, and their combined treatments, J. Wood Sci. 51 (2005) 148–153.

[27] L.K. Tolonen, P.A. Penttilä, R. Serimaa, A. Kruse, H. Sixta, The swelling and dissolution of cellulose crystallites in subcritical and supercritical water, Cellulose. 20 (2013) 2731–2744.

[28] T. Adschiri, S. Hirose, R. Malaluan, K. Arai, Noncatalytic Conversion of Cellulose in Supercritical and Subcritical Water, J. Chem. Eng. Japan. 26 (1993)

676–680.

[29] J.B. Sluiter, R.O. Ruiz, C.J. Scarlata, A.D. Sluiter, D.W. Templeton, Compositional analysis of lignocellulosic feedstocks. 1. Review and description of methods, J. Agric. Food Chem. 58 (2010) 9043–9053.

[30] D.W.T. Rippin, Chemical reaction engineering, 3rd ed., Wiley, New York, 1964. http://linkinghub.elsevier.com/retrieve/pii/000925096485017X. doi:10.1016/0009-2509(64)85017-X.

[31] O. Bobleter, Hydrothermal degradation of polymers derived from plants, Prog. Polym. Sci. 19 (1994) 797–841.

[32] T.H. Chilton, A.P. Colburn, Mass Transfer (Absorption) Coefficients: Prediction from Data on Heat Transfer and Fluid Friction, Ind. Eng. Chem. 26 (1934) 1183–1187.

[33] A.P. Colburn, A method of correlating forced convection heat-transfer data and a comparison with fluid friction, Int. J. Heat Mass Transf. 7 (1964) 1359–1384.

[34] J. Weisbach, Lehrbuch der Ingenieur- und Maschinen-Mechanik, Vol. 1. Theoretische Mechanik. (in German)., Theor. Mech. 1 (1845) 535.

[35] P.K. Swamee, A.K. Jain, Explicit equations for pipe-flow problems, J. Hydraul. Div. ASCE. 102 (1976) 657–664.

[36] D.A. Cantero, M. Dolores Bermejo, M. José Cocero, High glucose selectivity in pressurized water hydrolysis of cellulose using ultra-fast reactors, Bioresour. Technol. 135 (2013) 697–703.

[37] S. Deguchi, K. Tsujii, K. Horikoshi, Crystalline-to-amorphous transformation of cellulose in hot and compressed water and its implications for hydrothermal conversion, Green Chem. 10 (2008) 191–196.